Cadernos do Laboratorio Xeolóxico de Laxe
(2022) Vol. 44, 132–153
Instituto Universitario de Xeoloxía
Universidade da Coruña

ISSN: 0213-4497
eISSN: 2173-6936

Tourmalines in the Namacotche Li-Cs-Ta granitic pegmatite group, Mozambique: crystal chemistry and origin

Turmalinas en la pegmatita granítica de Li-Cs-Ta del Grupo Namacotche, Mozambique: cristalquímica y origen

Carlos A.A. LEAL GOMES[1], Ana M.R. NEIVA[2†]

[1]Lab2PT and Department of Earth Sciences, University of Minho, Gualtar, 4710-057 Braga, Portugal
[2]GeoBioTec, Department of Earth Sciences, University of Coimbra, 3030-790 Coimbra, Portugal
[†] Deceased

*Correspondent author: ensino2020.geo@gmail.com

https://doi.org/10.17979/cadlaxe.2022.44.0.9291
recibido: 25/10/2022 aceptado: 11/12/2022

Abstract

The field work, backscattered electron images and detailed microanalyses of three generations of tourmaline from the Namacotche LCT pegmatites allows de distinction between the compositional magmatic and hydrothermal tourmalines. The generation 1 occurs in the outer intermediate zone of the pegmatite. It consists of zoned crystals with an oscillatory inner core of foitite and schorl, an outer core of schorl and an Fe-rich fluor-elbaite rim. Unzoned Fe-rich fluor-elbaite crystals occur in the inner intermediate zone of the pegmatite. All the crystals are derived by fractionation of a (Al, Li, B)-rich pegmatite melt. However, the rim of zoned crystals and some compositions of unzoned crystals show evidence of hydrothermal fluids, as they plot outside the fractionation trends. The zoned fluor-elbaite crystals of the generation 2 are from the inner intermediate zone of the pegmatite. They have a pink core and a green rim. The rim has higher $^{Y}Fe^{2+}$, Na, F contents $^{Y}Fe^{2+}/(^{Y}Fe^{2+}+Li_{calc.})$ value and lower Si, ^{Y}Al, $Li_{calc.}$ and X-site vacancy

contents, X-vacancy/(Na+X-vacancy) value than the core. Both zones are hydrothermal. The rim is an overgrowth. The fluor-elbaite gemmy crystals of the generation 3 occur in sheared breccia blasts and clasts with a cookeite matrix. They depend mainly on the fluid-rich hydrothermal environment of low temperatures (280-150 ºC). Some from the cycle a may result from the dissolution of magmatic tourmaline crystals of the generation 1 from the sheared outer and inner intermediate zones of the pegmatite due to reaction with late fluids in chemical disequilibrium, followed by growth of tourmaline with low temperature hydrothermal fluids. The evolution from the cycle a to the cycle b and to the cycle c of the generation 3 implies that the hydrothermal reacting fluids were undergoing fractionation and becoming richer in Li and poorer in Fe^{2+} during the late hydrothermal crystallization of the pegmatites.

Key-words: foitite, schorl, fluor-elbaite, magmatic, hydrothermal, tourmaline dissolution, gems, LCT pegmatites, fluids

Resumen

El trabajo de campo, las imágenes de electrones retrodispersados y microanálisis detallados de tres generaciones de turmalina de las pegmatitas LCT de Namacotche permiten distinguir entre las turmalinas magmáticas y las hidrotermales. La generación 1 aparece en la zona intermedia exterior de la pegmatita. Consiste en cristales zonados con un núcleo interno oscilante de foitita y esquisto, un núcleo externo de esquisto y un borde de fluor-elbaita rico en Fe. En la zona intermedia interior de la pegmatita aparecen cristales no zonados de fluor-elbaita ricos en Fe. Todos los cristales derivan del fraccionamiento de un fundido pegmatítico rico en Al, Li y B. Sin embargo, el borde de los cristales zonados y algunas composiciones de cristales no zonados muestran evidencias de fluidos hidrotermales, ya que trazan fuera de las tendencias de fraccionamiento. Los cristales zonados de fluor-elbaita de la generación 2 proceden de la zona intermedia interna de la pegmatita. Tienen un núcleo rosa y un borde verde. El borde tiene mayor contenido en YFe2+, Na, F (YFe2+/(YFe2++Licalc.)) y menor contenido en Si, YAl, Licalc. y vacantes X, vacantes X/(Na+X-vacantes) que el núcleo. Ambas zonas son hidrotermales. El borde es un sobrecrecimiento. Los cristales geminados de fluor-elbaita de la generación 3 aparecen en clastos de brechas cizalladas y en clastos con matriz de cookeita. Dependen principalmente del ambiente hidrotermal rico en fluidos de bajas temperaturas (280-150 ºC). Algunos del ciclo a pueden ser el resultado de la disolución de cristales magmáticos de turmalina de la generación 1 de las zonas cizalladas externa e interna intermedia de la pegmatita debido a la reacción con fluidos tardíos en desequilibrio químico, seguida del crecimiento de la turmalina con fluidos hidrotermales de baja temperatura. La evolución del ciclo a al ciclo b y al ciclo c de la generación 3 implica que los fluidos hidrotermales reaccionantes estaban sufriendo fraccionamiento y haciéndose más ricos en Li y más pobres en Fe2+ durante la cristalización hidrotermal tardía de las pegmatitas.

Palabras clave: foitita, chorlo, elbaíta fluorada, magmático, hidrotermal, disolución de la turmalina, gemas, pegmatitas de LCT, fluidos

1. INTRODUCTION

Some studies on gem tourmaline have been published (e.g. PERETTI *et al*. 2009 and references therein; SIMMONS, 2014; WILSON, 2014). Gem tourmaline occurs in some pegmatites, particularly in miarolitic cavities or pockets (Simmons *et al*., 2012). Late-stage pockets supply most gem tourmaline (SIMMONS, 2014). The most common species is elbaite, followed by liddicoatite (SIMMONS *et al*., 2001; DIRLAM *et al*., 2002). The gem elbaite commonly occurs in Li-bearing pegmatites (WILSON, 2014). In the LCT pegmatites, as the crystallization proceeds from the wall zone to late stage pockets formation, the Fe content in the melt decreases and if the melt contains enough B and Al and sufficient enrichment of Li, the sequence of tourmaline crystallization is from schorl to elbaite (SIMMONS, 2014). In the final stages of crystallization or late-stage alteration products, X-site deficient tourmaline may from by a reaction of fluids with earlier formed tourmaline, leaching alkalis from the tourmaline or dissolving it, followed by re-precipitation of an alkali-deficient tourmaline (DUTROW & HENRY, 2000; SIMMONS, 2014).

Tourmaline fibers nucleate in preexisting tourmaline, but also in other minerals. Some fibers are homogeneous, but others are chemically zoned. The cat's eye tourmaline is rare and a consequence of tourmaline's fibrous habit. Most tourmaline fibers form late e.g. at the end of the tourmaline crystallization sequence in a pegmatite pocket or in a hydrous fluid-rich fracture system. In general, the composition of the interactive fluid phase controls the chemical compositions of the fibers. Most of them develop at relatively low temperature (DUTROW & HENRY, 2016 and references therein).
Tourmaline is an important accessory mineral of the Namacotche granitic pegmatites containing gemmy tourmaline crystals and a few cat's eye. A detailed chemical study of tourmalines from these pegmatites was undertaken to provide information on the formation conditions particularly of gem tourmalines.

2. ANALYTICAL METHODS

Chemical compositions and backscattered electron images were obtained using a Cameca SX 100 electron microprobe at the Department of Earth Sciences, University of Manchester, U.K. The electron microprobe operated at 15 kV accelerating voltage and 20 nA beam current. Detection limits (3s) above mean background were < 0.03 wt.% oxide, except for F (0.1 wt.%), with counting times of 80 s. The trace elements Cr, V, Zn, Cu and Pb were not detected.

The general formula of HAWTHORNE & HENRY (1999) and BOSI & LUCHESSHI (2007) and HENRY *et al*. (2011) are used. Structural formulae are calculated on the basis of 31 anions using the Microsoft Excel™ worksheet of TINDLE *et al*. (2002). Boron is assumed to be stoichiometric. All Fe and Mn are assumed to be divalent and Li is assigned to the Y site. Li, OH and H_2O are calculated by stoichiometry. The tourmaline

classification of HAWTHORNE & HENRY (1999) and HENRY *et al*. (2011) are used.

3. GEOLOGICAL SETTING

Namacotche gem-bearing pegmatites are located in the Alto Molocué region of Zambezia Administrative Province of Mozambique. Hierarchy of regional distribution of pegmatites according to ČERNÝ (1982) is described in LEAL GOMES *et al*. (2008) (Fig. 1). The first order unit may be called Zambezian Pegmatite Province, which shows a concentrically zoned distribution of the different pegmatite families, where LCT types predominate at the core domain in the Alto Ligonha Pegmatite District. This aureolar space arrangement of the various mineralogical and geochemical signatures seems to be correlated with a superposition of terraines of different structural and lithological levels. These coincide locally with overthrusted mantles originated from lithotypes of variable primitive nature and age. The pegmatite distribution is strongly influenced by the setting of over-thrust related to strike-slip structures.

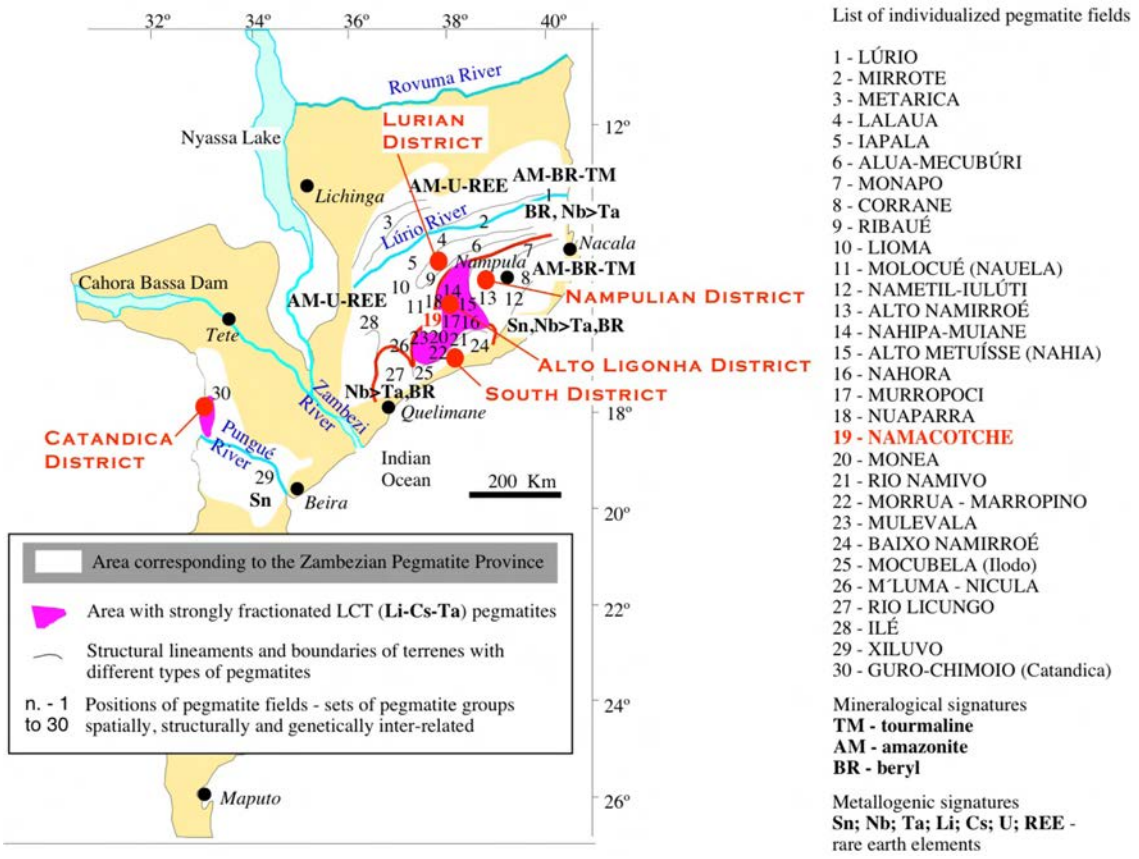

Figure 1. Location of the Namacotche pegmatite field in the context of the regional distribution of Mozambican Pegmatites.

In the Central District of Alto Ligonha, the Namacotche Field is located in a central position, where the main geological formations and regional rock types are illustrated in Fig. 2 and systematized as follows:

- *Amphibolite gneisses and other mafic gneisses – Molocué complex (AG)*

The metabasites of the Molocué Group are dominated by amphibolites, but include metagabbros, amphibole-epidote-pyroxene-garnet gneisses, as well as talc and chlorite schists, anthophyllite schists, epidote-rich rocks and metapyroxenites to meta-dunites (AQUATER, 1983). Layered greenish black amphibolites are interbedded with quartz-feldspathic gneisses. Quartzites usually occur nearby. The layered nature of these units suggests the partially contemporaneous deposition of protolithic felsic, metavolcanic rocks and some mafic lavas, with the deposition of the sedimentary succession. These are the host-rocks of the Namacotche main pegmatite

Some segregation-ptygmatic quartz veins are parallel to the banding, both being deformed in distinct events. In thin section, secondary holmquistite was identified in some metasomatized amphibolite outcropping at the contact with highly fractionated LCT pegmatites. Oriented amphibole and locally pyroxene define a tectono-metamorphic, planar S1 fabric of aligned amphibole and plagioclase.

- *Undifferentiated – metapelite and metapsammite gneisses with inter-layered subordinated calc-silicate rocks (UMMG)*

Still in the Molocué Group some biotite gneisses grade into muscovite-biotite schists (metapsamites and metapelites) and gneisses (metarhyolites) (AQUATER, 1983). Metamorphic grade varies from amphibolitic to sillimanitic.

Mica schists are poorly exposed and comprise predominantly muscovite-biotite and quartz, plagioclase, sillimanite and epidote, apatite and tourmaline as accessory minerals.

- *Leucocratic quartz-feldspar gneisses – Mamala Gneisses (LG)*

Based on textures, grain size and the proportions of biotite, pyroxene and magnetite, AQUATER (1983) isolated the Mamala gneisses. These formations are interpreted as protolithic interlayered metarhyolitic lavas and pyroclastic rocks, metamorphosed into fine- to medium-grained, dominantly leucocratic gneisses, with a typical granitic composition – with similar proportions of microcline, plagioclase and quartz, and minor biotite, rare garnet and clinopyroxene.

- *Layered migmatitic biotite gneisses – Mocuba Complex (MBG)*

The heterogeneous banded gneisses are inter-layered with variable amounts of foliation-parallel quartz-feldspar leucosomes. The palaeosome layers usually have granodioritic, tonalitic or dioritic compositions.

The leucosomes are consistently equigranular and include quartz, feldspar and minor biotite and hornblende. The migmatitic melt veins are significantly coarser-grained and characterized by a granoblastic texture typical of metamorphic recrystallization. The

earliest melt veins may be related to the Kibaran DI/MI event. They form rootless intrafolial folds within the gneissic layering. The Pan-African D2 deformation was also accompanied by partial melting, generating S2-parallel stromatic leucosomes. Post-dating phases of migmatisation are expressed as cross-cutting, locally ptygmatically folded, melt veins and more diffuse leucosomes. Multiple generations of parallel to discordant aplite to pegmatite veins and dykes may be present.

Within the main cartographic unit, granitoid orthogneisses do occur, containing infolded layers, discontinuous lenses and boudins of melanocratic amphibolites and biotite-rich rocks that are interpreted as pre-tectonic mafic dykes (AQUATER, 1983).

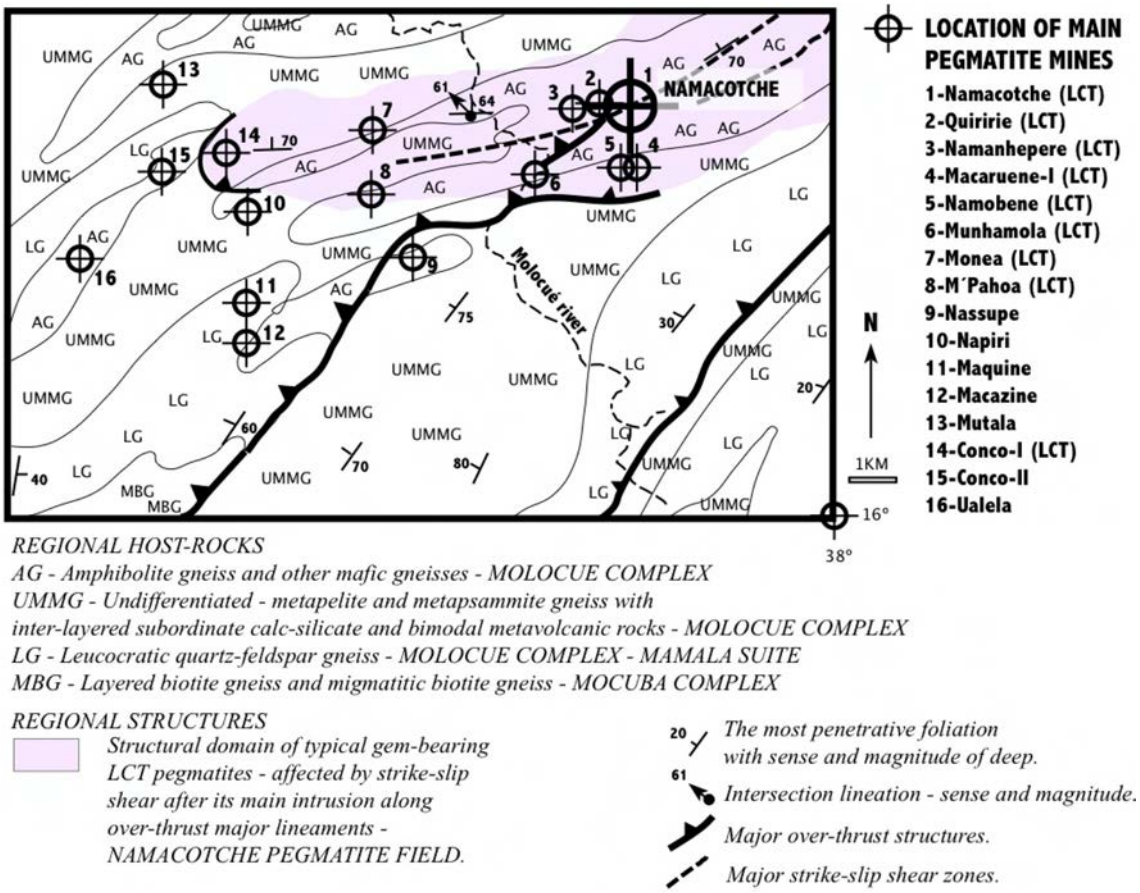

Figure 2. Simplified geological map of the SW Sector of the Namacotche pegmatite field enhancing the location of the Namacotche pegmatite mine were tourmaline samples were collected.

4. STRUCTURE OF THE NAMACOTCHE PEGMATITE GROUP

Namacotche pegmatites are emplaced along a major shear corridor in a metasedimentary to metavolcanic sequence of amphibolitic host-rocks (Fig. 2). The larger pegmatites are located in pull-a-part domains associated with tangential shear motion in major over-thrust structures. The more evolved mineral assemblages as well as multipulse remobilization assemblages and brecciated, hydrothermally replaced volumes, are also

located near the more disturbed compartments, which gradually evolved to transcurrent strike-slip shear.

In the late, shear-opened system, the hydrothermal activity might have promoted the inward migration of outer contaminated fluids as, inside cookeite assemblages and some late vanadium minerals do occur, accompanying the last Bi minerals. Besides bismite, sphaerobismoite and bismutite with rare accessory electrum, the Namacotche pegmatite group presents the rare minerals, bismutostibiconite, clinobisvanite and pucherite, occuring in complex aggregates, entrapped in the last transtenssive to transpressive depositional sites in bismite/bismuthite hosts with some beyerite (LEAL GOMES *et al*., 2006). Vanadium could be removed from amphibolite neighbors. In Fig. 3 the most structurally complex pegmatite compartments are surrounded by amphibolite enriched in spinels, namely coulsonite, which is a probable primitive source of vanadium.

Outwards, pegmatite-emanated fluids caused holmquistite replacement of earlier contiguous amphiboles and some tourmalinization at the most pelitic host-rocks.

The structural constraints revealed in Fig. 3 could explain the cyclical reactivation and late regeneration of low temperature hydrothermal assemblages that include gem tourmaline.

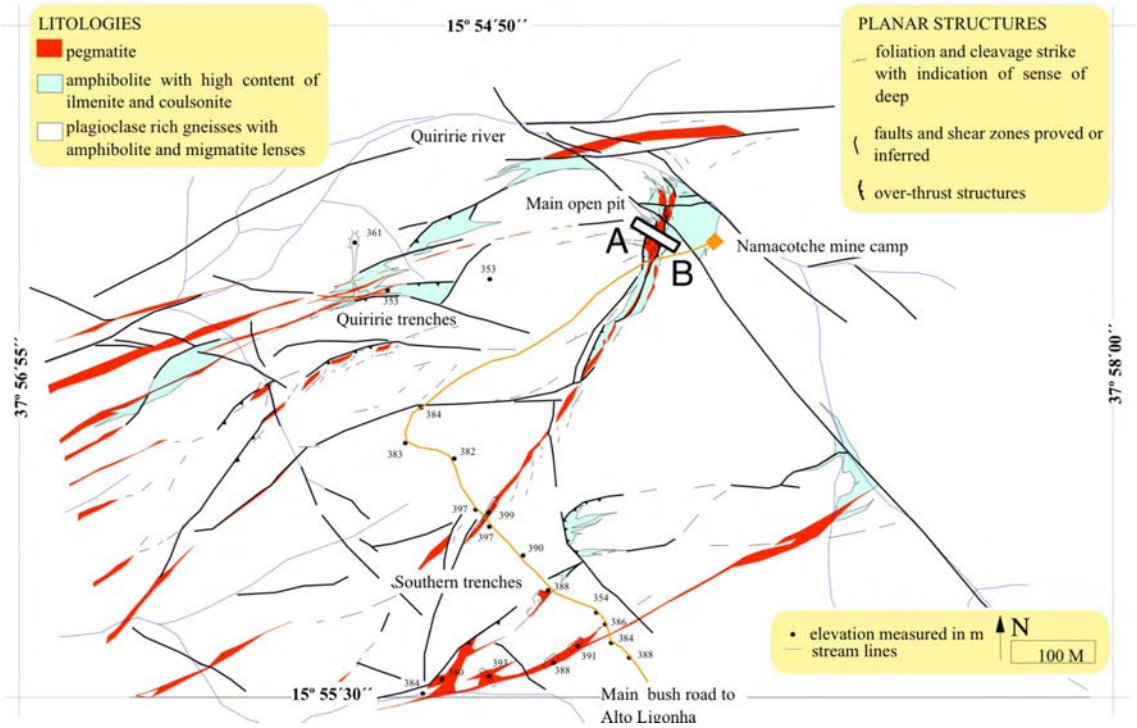

Figure 3. Structure of the Namacotche pegmatite group with location of A-B sketched general cross-section, which is presented in Fig. 4.

5. STRUCTURE AND MINERALOGY OF THE NAMACOTCHE PEGMATITE

All the observed pegmatites are heterogeneous, strongly fractionated, with high Li and Ta contents and extremely high Cs contents. According to the classification of ČERNÝ

& ERCIT (2005), the Namacotche granitic pegmatites belong to the Rare Element (REL) class, REL-Li subclass, complex type and spodumene - lepidolite - elbaite subtype. At the major pegmatite body exposed at the main open pit (Fig. 3), the pale colored gemstones, morganite (pink Cesian-beryl), kunzite-triphane (spodumene) and elbaite (tourmaline), are hosted in dilation cavities (tension gashes), predominantly at the inner intermediate zones. These minerals coat the open spaces of the last fractionated and layered cleavelandite units and occur inside replacement units, and sheared related breccias (Fig. 4). Mineralogy and the inner distribution of mineral assemblages are described in Table 1. The best gem pockets seem to be linked to late re-precipitation stages of subsolidus replacement associated with multipulse shearing.

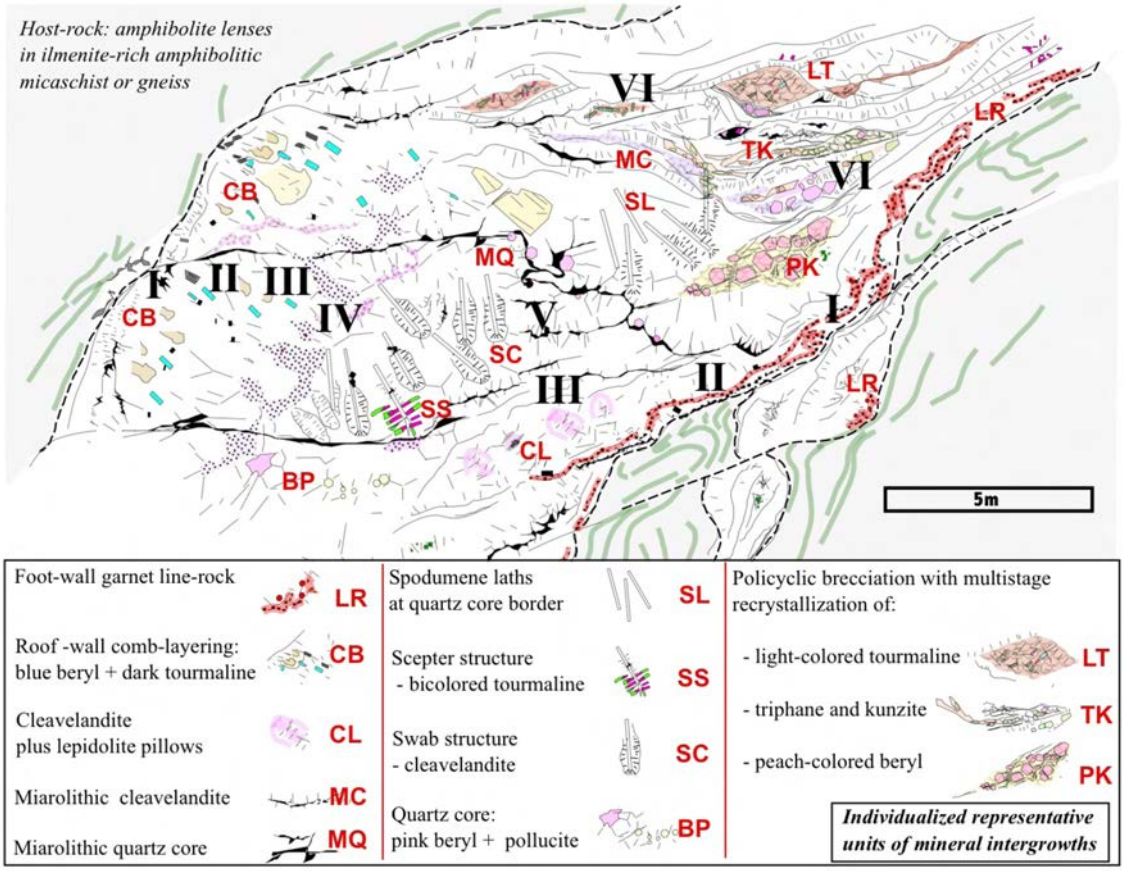

Figure 4. Integrative sketch profile – traverse 2d, vertical, WNW-SSE, located as A-B in Fig. 3 and exposed to the North - showing the inner structure and the distribution of individualized textural cells including peculiar intergrowths with tourmaline. Inner zoning is composed by: I – wall zone; II – border zone; III – outer intermediate zone; IV – inner intermediate zone; V – core zone (quartz, spodumene and/or cleavelandite); VI – late units with dominant cleavelandite, in breccias and tensions gashes filled by cookeite, late lepidolite and hydrothermal clay minerals, surrounding more or less corroded and recrystallized tourmaline clasts. Note: the same zone references are used in Table 1.

Cookeite and other clay minerals as well as lepidolite are frequently intergrown with gem minerals. They occupy late tension gashes and fractures and form hydrothermal breccia spots with gem clasts and blasts, which are cemented by clay mineral groundmasses. BRAGA *et al*. (2008) reported the following significant clay occurrences:

- late cleavelandite units with porous cookeite masses and clays as fractures infilling;
- pseudomorphic lepidolite and clay after formed primary spodumene and tourmaline;
- morganite (re-crystallized Cesian-beryl) and gem spodumene associated with cookeite and clays in porous cookeite formed after primary spodumene laths;
- gem tourmaline of second generation in veins and breccias with cookeite and other clay minerals.

Table 1. Cheklist for the main mineral locations in assemblages typical of the Namacotche pegmatite zoning.

MINERALS	I roofwall	I footwall	II	III	IV	V	VI
tourmaline	+	+	+	+	+		+
beryl	+				+	+	+
spodumene					+		+
topaz					+	+	
pollucite						+	
lepidolite				+	+		
polylithionite				+			
coockeite							+
clay minerals							+
Mn-almandine		+					
spessartite					+	+	
Fe - columbite	+	+	+				
Mn - tantalite				+	+	+	
Sb - tantalite						+	+
Ba - microlite				+			
U, Pb - microlite							+
F, Na - microlite				+	+		
gahnite		+	+				
rutile	+	+				+	
bazzite						+	
vigezzite						+	+
magnetite		+					
F-apatite				+	+	+	
OH-herderite					+		
amblygonite - montebrasite					+	+	
bismuthite					+	+	+
malachite					+	+	
bismite							+
sphaerobismoite							+
bismutostibiconite							+
clinobisvanite							+
pucherite							+
beyerite							+
quartz	+	+	+	+	+	+	
albite	+	+	+	+	+	+	+
microcline	+		+				

I – wall zone; II – border zone; III – outer intermediate zone; IV – inner intermediate zone; V – core zone (quartz, spodumene and/or cleavelandite); VI – late units with dominant cleavelandite, in breccias and tensions gashes filled by cookeite, late lepidolite and hydrothermal clay minerals. The zones are shown in Fig. 4.

Considering the clay mineralogy, the comprehensive assemblage may be established as follows: cookeite - irregularly interstratified cookeite-smectite - beidellite + montmorillonite - interstratified illite-smectite - kaolinite.

According to BRAGA *et al*. (2008) and LEAL GOMES (2003a, b) disequilibrium of the primary paragenesis and re-crystallization of some of their accessory minerals at low temperatures are considered to be responsible for the precipitation of the gemstones and the enhancement of its gem quality. A 280 to 150 ºC thermal range is attributed to this late hydrothermal stage on the basis of fluid inclusion studies concerning cesian-beryl, hyaline quartz, spodumene and elbaite. The association of cookeite + smectite was considered a paragenetic guide to the location of low temperature gemstone spots.

6. INNER PARAGENESIS AND TOURMALINE MODE OF OCCURRENCE

Primary tourmalines include the following modes of occurrence: contact zone – black tourmaline sprayed crystals; border zone – black tourmaline massive aggregates and needle like crystals; outer-intermediate zone – black tourmaline and dark green to grey crystals (Fig. 5, A1); inner-intermediate zone – scepter like aggregates light green to pink (Fig. 5, A2); miarolithic, cleavelandite-rich units – red crystals.

Recrystallized tourmalines occur at policyclic remobilization units as: green to dark green and translucent isolated relict crystals (Fig. 5, C1); dark green to light green and etched clustered crystals (Fig. C2); light pink corroded and acroite to light blue corroded recrystallized aggregates (Fig. 5, C3, C4).

As illustrated in Fig. 4, primary tourmalines can be attributed to a sequence of inner fractionation since border zone to quartz core, occurring in persistent proximity to cleavelandite comb layers and terminations of spodumene laths.

Late stage or secondary tourmalines might be considered the result of remobilization and hydrothermal recrystallization in multistage disequilibria and collapse of earlier tourmaline assemblages, specially, those of primary and fractional mineral assemblages. From a textural point of view, they seem to be equivalent to clasts or blasts of late breccias located at pull-a-part dilational volumes of over-thrust tangential displacement inside the most deformed and replaced pegmatite compartments.

Several cycles of secondary tourmaline equilibrium are texturally discriminated. Some are related to the same paragenetic generation type of alkaline beryl and gem spodumene, although spodumene and beryl seem to be reequilibrated only once and at the immediate proximity of the primary expression of the same mineral species.

The highest gem quality of the tourmaline is achieved when it occurs as breccia clasts of several generations in a matrix of clay minerals with predominant coockeite and some lepidolite (BRAGA *et al*., 2008). The evolved breccia clasts are deposited in typical hydrothermal conditions inside the dilational sites associated with transpressive tangential motion of cleavelandite panels formed during late stage synkinematic crystal growth. Voids generated during the early stage of the overthrust movement collect tourmalines of the early remobilization cycle. The following overthrust readjustments controlled the successive cycles of tourmaline redeposition – the last hydrothermal

activity being responsible for corrosion and etching of tourmalines of primary origin and earlier clasts, which led to a general cleaning by crystal defects leaching.

Figure 5. Textural, morphological and chromatic diversity of primary and secondary clastic tourmalines and associated minerals. A – primary tourmalines: A1 – early black to dark blue-green tourmaline from the outer intermediate zone; A2 – light-pink to light-green water-mellon tourmaline from the inner intermediate zone. B - clastic, corroded and recrystallized minerals from the late breccias and tension gashes: B1 – gemmy and light-colored tourmaline clasts in cookeite-goethite matrix; B2 – recrystallized triphane type spodumene in an illite, illite-smectite, cookeite-smectite mixed-layers, beidellite, montmorillonite and kaolinite groundmass; B3 – recrystallized morganite type Cesian-beryl in a matrix of cookeite and lepidolite. C - secondary tourmalines with good gem quality, attributed to recrystallization during different episodes of multistage shear and multipulse hydrothermal remobilization: C1 – remnant clasts of early corroded generation; C2 – recrystallized and surface smoothed elongated crystals with the best gem quality; C3 – the last pale blue recrystallized crystals; C4 – pale pink crystals of the same generation.

7. CHEMICAL COMPOSITIONS OF TOURMALINE CRYSTALS

Representative chemical analyses of studied zoned and unzoned crystals of the tourmaline generations from the Namacotche pegmatites are given in Tables 2 and 3. Most tourmaline compositions belong to the Na alkali group, but some compositions from the generation 1 belong to the vacancy group (Fig. 6). The largest variety of compositions ranging from foitite to schorl and Fe-rich fluor-elbaite was found in crystals from the

generation 1 (Fig. 7a). Crystals of the generations 2 and 3 are of fluor-elbaite.

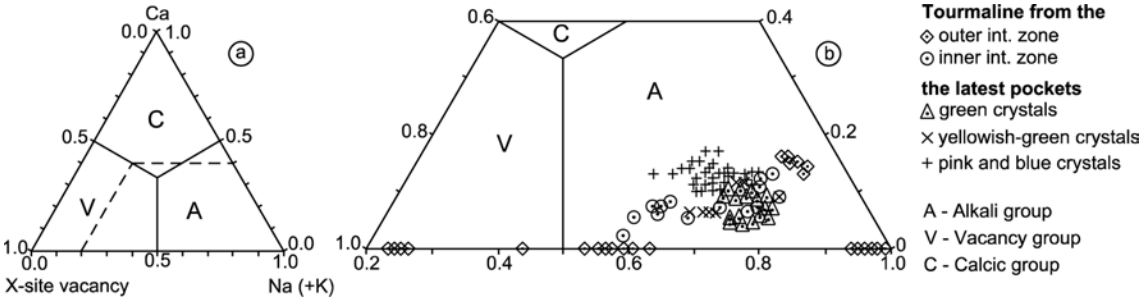

Figure 6. Tourmaline compositions from the Namacotche granitic pegmatites, Mozambique; a. Classification of the principal tourmaline groups based on the X-site occupancy (Hawthorne & Henry, 1999; Henry *et al*., 2011), showing the location of diagram b; b. Generation 1 plots in the vacancy group and alkali group, but the other generations plot in the alkali group.

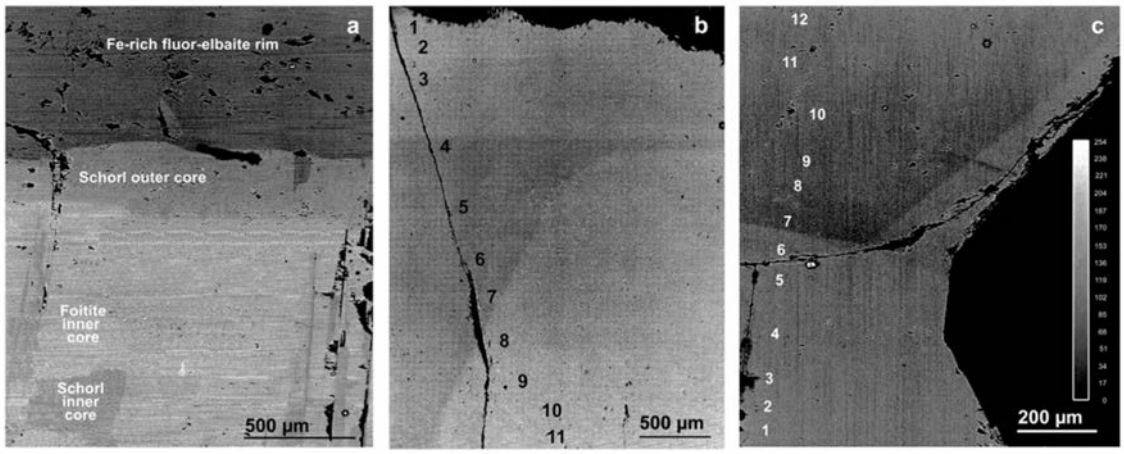

Figure 7. Backscattered images of zoned tourmaline crystals from the Namacotche granitic pegmatites, Mozambique. a. A mainly progressive zoned crystal with a foitite and schorl inner core, to a schorl outer core and a Fe-rich fluor-elbaite rim from the generation 1; b. A slightly oscillatory zoned fluor-elbaite crystal of the cycle a from the generation 3. c. A progressively zoned fluor-elbaite crystal of the cycle b from the generation 3.

7.1. Generation 1

The zoned tourmaline crystals of the generation 1 are from the outer intermediate zone of the pegmatite. They are black to dark blue-green in color (Fig. 5, A1).

In backscattered (BSE) images they reveal a lighter inner core of foitite, alternating with a grey inner core of schorl showing a gradational interface. A grey outer core of schorl presents a gradational transition to the foitite inner core. A dark rim of Fe-rich fluor-elbaite shows a sharp contact with the schorl outer core (Fig. 7a).

Grey (in BSE), unzoned, Fe-rich fluor-elbaite crystals in equilibrium, occur at the outer intermediate zone of the pegmatite, but similar crystals in disequilibrium are from the inner intermediate zone.

Table 2 . Some representative electronic microprobe analyses of tourmaline crystals of from the Namacotche granitic pegmatites, Mozambique.

		Outer intermediate zone					Inner intermediate zone				
		Progressive zoning					Unzoned	Unzoned		Zoned crystals	
		Inner	Core	Outer core	Rim		crystal	unzoned	crystal	Pink core	Green rim
SiO_2		36.45	36.42	36.42	36.73	37.12	36.84	36.10	36.63	38.89	38.04
TiO_2		—	—	—	—	—	—	0.05	0.07	0.02	0.02
B_2O_3*		10.45	10.49	10.50	10.66	10.69	10.61	10.60	10.69	11.10	10.96
Al_2O_3		34.41	34.86	35.02	35.81	36.11	35.33	36.26	36.79	39.70	38.65
FeO		13.24	11.73	11.12	7.56	6.25	8.46	7.15	5.42	0.16	1.83
MnO		0.35	0.36	0.52	1.02	1.03	0.37	1.59	2.22	1.60	2.35
MgO		0.38	0.19	0.07	0.09	0.11	0.08	0.05	0.06	0.01	0.03
Li_2O*		0.40	0.71	0.81	1.43	1.62	1.44	1.30	1.41	2.27	1.90
CaO		—	—	—	0.93	0.04	0.01	0.65	0.59	0.36	0.34
Na_2O		0.82	1.63	1.85	2.37	3.09	3.07	2.42	2.33	2.02	2.44
K_2O		—	0.01	—	0.01	0.02	0.01	0.02	0.01	—	0.01
H_2O*		3.60	3.40	3.30	3.11	2.86	2.89	3.01	3.07	3.23	3.09
F		—	0.47	0.68	1.19	1.75	1.61	1.36	1.30	1.26	1.46
Cl		—	—	—	—	—	0.02	—	0.01	—	—
Sum		100.10	100.27	100.29	100.91	100.69	100.74	100.56	100.60	100.62	101.12
O≡F		—	0.20	0.29	0.50	0.74	0.68	0.57	0.55	0.53	0.61
Total		100.10	100.07	100.00	100.41	99.95	100.06	99.99	100.05	100.09	100.51
T	Si	6.064	6.034	6.028	5.989	6.037	6.036	5.918	5.957	6.091	6.030
	Al	—	—	—	0.011	—	—	0.082	0.043	—	—
B		3.000	3.000	3.000	3.000	3.000	3.000	3.000	3.000	3.000	3.000
Z	Al	6.000	6.000	6.000	6.000	6.000	6.000	6.000	6.000	6.000	6.000
Y	Al	0.748	0.807	0.832	0.870	0.921	0.822	0.924	1.009	1.329	1.220
	Ti	—	—	—	—	—	—	0.006	0.009	0.002	0.002
	Mg	0.094	0.047	0.017	0.022	0.027	0.020	0.012	0.015	0.002	0.007
	Mn	0.049	0.051	0.073	0.141	0.142	0.051	0.221	0.306	0.212	0.316
	Fe^{2+}	1.842	1.625	1.539	1.031	0.850	1.159	0.980	0.737	0.021	0.243
	Li*	0.267	0.470	0.539	0.936	1.060	0.948	0.857	0.924	1.434	1.212
	Ca	—	—	—	0.162	0.007	0.002	0.114	0.103	0.060	0.058
	Na	0.265	0.524	0.594	0.749	0.974	0.975	0.769	0.735	0.613	0.750
	K	—	0.002	—	0.002	0.004	0.002	0.004	0.002	—	0.002
	□	0.735	0.474	0.406	0.087	0.015	0.021	0.113	0.160	0.327	0.190
V+Wsite:	OH	4.000	3.753	3.643	3.383	3.096	3.156	3.291	3.326	3.374	3.266
Vsite:	OH	3.000	3.000	3.000	3.000	3.000	3.000	3.000	3.000	3.000	3.000
Vsite:	O	—	—	—	—	—	—	—	—	—	—
Wsite:	OH	1.000	0.753	0.643	0.383	0.096	0.156	0.291	0.326	0.374	0.266
Wsite:	F	—	0.247	0.357	0.617	0.904	0.838	0.709	0.671	0.626	0.734
Wsite:	Cl	—	—	—	—	—	0.006	—	0.003	—	—
Wsite:	O	—	—	—	—	—	—	—	—	—	—
V, Wsite:	total	4.000	4.000	4.000	4.000	4.000	4.000	4.000	4.000	4.000	4.000
Colour		Lighter grey	Darker grey	Grey	Black $^{Y}Fe^{2+}$-rich	Black	Grey $^{Y}Fe^{2+}$-rich	Grey	Darker grey	Darker grey	Lighter grey
in BSE		Foitite	Schorl	Schorl	Fluor-elbaite	Fluor-elbaite	Fluor-elbaite	Fluor-elbaite		Fluor-elbaite	

Compositions in weight % and structural formula based on 31 anions (O, OH, F) in atoms per formula. * Amount inferred from considerations of stoichiometry. — Not detected. BSE – Backscattered image.

The compositions of all of these crystals define linear trends from foitite to schorl and Fe-rich fluor-elbaite showing decrease in $^{Y}Fe^{2+}/(^{Y}Fe^{2+}+Li_{calc.})$, X-vacancy/(Na + X-vacancy) values, $^{Y}Fe^{2+}$, X-site vacancy contents and increase in $Li_{calc.}$ content (Figs. 8, 9). However, in these diagrams, the rim composition of zoned crystals (Fig. 7a) and a few analyses of crystals in disequilibrium plot outside these trends and have lower $^{Y}Fe^{2+}/(^{Y}Fe^{2+}+Li_{calc.})$ value and $^{Y}Fe^{2+}$ content than the other Fe-rich fluor-elbaite compositions (Figs. 8, 9). The rim has the highest Li content (Figs. 7a, 9a). The crystals from this generation 1 present the largest ranges of elements. Schorl from the outer core has lower Mg and Fe^{2+} contents and higher Mn, $Li_{calc.}$, Na and F contents than schorl from the inner core (Fig. 7a, Table 2). In general, from foitite to schorl and Fe-rich fluor-elbaite,

$^{Y}Fe^{2+}/(^{Y}Fe^{2+}+Li_{calc.})$, X-vacancy/(Na+X-vacancy), X-site vacancy values and $^{Y}Fe^{2+}$ content decrease and Mn, $Li_{calc.}$, Na, F contents increase (Figs. 7a, 8, 9, Table 2). The crystals are oscillatory zoned in the inner core, but progressively zoned from the inner core to the outer core and rim. The compositional evolution is best described by the exchange vectors (Fe_2) $(LiAl)^{-1}$, (NaLi) $(\square Fe)^{-1}$ and $F(OH)^{-1}$ (Fig. 9).

Table 3. Some representative electron microprobe analyses of fluor-elbaite crystals of the generation 3 from the Namacotche granitic pegmatites, Mozambique

		The Latest pockets										
		Green			Yellowish-green			Pink				
						Crystal with cat's eye effect					Blue	
			Oscillatory zoned			Progressively zoned			Reversely zoned			
		Unzoned	Darker zone	Lighter zone	Unzoned	Darker core	Lighter rim	Unzoned	Lighter core	Darker rim	Unzoned	Unzoned
SiO_2		37.96	37.95	37.51	37.28	37.80	37.69	38.48	38.37	38.23	38.37	38.99
TiO_2		0.04	0.02	0.01	0.02	0.02	0.02	—	—	0.02	0.01	—
B_2O_3*		10.91	10.94	10.91	10.89	10.98	10.89	11.02	10.99	10.98	10.99	11.12
Al_2O_3		38.01	38.71	38.86	39.09	39.35	38.36	39.02	38.71	38.97	38.71	39.53
FeO		2.51	2.12	2.50	1.53	1.29	1.48	0.09	0.37	0.24	0.37	0.03
MnO		1.78	1.64	1.82	2.41	2.25	2.55	1.90	2.48	2.38	2.48	1.10
MgO		0.05	0.05	0.07	0.02	0.03	0.02	—	0.01	—	0.01	0.01
Li_2O*		1.98	1.94	1.76	1.81	1.87	1.93	2.34	2.20	2.17	2.20	2.49
CaO		0.55	0.44	0.32	0.53	0.43	0.63	1.01	0.69	0.77	0.69	0.81
Na_2O		2.39	2.35	2.47	2.32	2.35	2.39	2.05	2.18	2.11	2.18	2.05
K_2O		0.01	—	—	—	0.03	0.01	—	—	—	—	—
H_2O*		3.08	3.12	3.09	3.02	3.17	3.07	3.11	3.10	3.11	3.10	3.21
F		1.44	1.37	1.42	1.56	1.30	1.45	1.47	1.46	1.44	1.46	1.31
Cl		—	0.01	—	—	—	0.01	—	—	—	—	—
Sum		100.71	100.66	100.74	100.48	100.87	100.50	100.49	100.56	100.42	100.57	100.65
O≡F		0.61	0.58	0.60	0.66	0.55	0.61	0.62	0.61	0.61	0.61	0.55
Total		100.10	100.08	100.14	99.82	100.32	99.89	99.87	99.95	99.86	99.96	100.10
T	Si	6.049	6.028	5.977	5.950	5.985	6.015	6.067	6.069	6.049	6.069	6.096
	Al	—	—	0.023	0.050	0.015	—	—	—	—	—	—
B		3.000	3.000	3.000	3.000	3.000	3.000	3.000	3.000	3.000	3.000	3.000
Z	Al	6.000	6.000	6.000	6.000	6.000	6.000	6.000	6.000	6.000	6.000	6.000
Y	Al	1.138	1.247	1.276	1.304	1.328	1.215	1.250	1.217	1.268	1.217	1.285
	Ti	0.005	0.002	0.001	0.002	0.002	0.002	—	0.001	0.002	0.001	—
	Mg	0.012	0.012	0.017	0.005	0.007	0.005	—	0.002	—	0.002	0.002
	Mn	0.240	0.221	0.246	0.326	0.302	0.345	0.254	0.332	0.319	0.332	0.146
	Fe^{2+}	0.334	0.282	0.333	0.204	0.171	0.198	0.012	0.049	0.032	0.049	0.004
	Li*	1.271	1.236	1.127	1.159	1.190	1.235	1.484	1.399	1.379	1.399	1.563
X	Ca	0.094	0.075	0.055	0.091	0.073	0.108	0.171	0.117	0.131	0.117	0.136
	Na	0.738	0.724	0.763	0.718	0.721	0.739	0.627	0.669	0.647	0.669	0.621
	K	0.002	—	—	—	0.006	0.002	—	—	—	—	—
	□	0.166	0.201	0.182	0.191	0.200	0.151	0.202	0.214	0.222	0.214	0.243
V+Wsite: OH		3.272	3.307	3.283	3.210	3.348	3.263	3.267	3.270	3.279	3.267	3.350
Vsite:	OH	3.000	3.000	3.000	3.000	3.000	3.000	3.000	3.000	3.000	3.000	3.000
Vsite:	O	—	—	—	—	—	—	—	—	—	—	—
Wsite:	OH	0.272	0.307	0.283	0.210	0.348	0.263	0.267	0.270	0.279	0.267	0.350
Wsite:	F	0.728	0.690	0.717	0.790	0.652	0.734	0.733	0.730	0.721	0.733	0.650
Wsite:	Cl	—	0.003	—	—	—	0.003	—	—	—	—	—
Wsite:	O	—	—	—	—	—	—	—	—	—	—	—
V, Wsite:	total	4.000	4.000	4.000	4.000	4.000	4.000	4.000	4.000	4.000	4.000	4.000
Colour in BSE		Light grey	Darker grey	Lighter grey	Grey	Darker grey	Lighter grey	Light grey	Very light grey	Light grey	Dark grey	Light grey

Compositions in weight % and structural formula based on 31 anions (O, OH, F, Cl) in atoms per formula. * Amount inferred from considerations of stoichiometry. — Not detected. BSE – Backscattered image.

7.2. Generation 2

The tourmaline crystals of the generation 2 are typical of the pegmatite inner intermediate zone. They consist of a pink fluor-elbaite core and a green fluor-elbaite rim (Figs. 5A2, 8, Table 2), similar to the gem variety, watermelon. The rim has higher $^{Y}Fe^{2+}$, Na, F contents and $^{Y}Fe^{2+}/(^{Y}Fe^{2+}+Li_{calc.})$ value and lower Si, ^{Y}Al, $Li_{calc.}$, X-site vacancy contents and X-vacancy/(Na+X-vacancy) value than the core (Figs. 8, 9, 10; Table 2). A gap occurs between the compositions of core and rim. The variability within this generation 2 compositions is better explained by the $(NaFe)(Al)^{-1}$ vector (Fig. 9b). These crystals have $^{Y}Fe^{2+}/(^{Y}Fe^{2+}+Li_{calc.})$ values of 0.21-0.01, which are lower than those for generation 1. Core and rim have higher ^{Y}Al, Li, X-site vacancy contents and X-vacancy/(Na+X-vacancy) values and lower Mg, $^{Y}Fe^{2+}$, F contents and $^{Y}Fe^{2+}/(^{Y}Fe^{2+}+Li_{calc.})$ value than the Fe-rich fluor-elbaite in equilibrium from the generation 1 (Figs. 8, 9; Table 2).

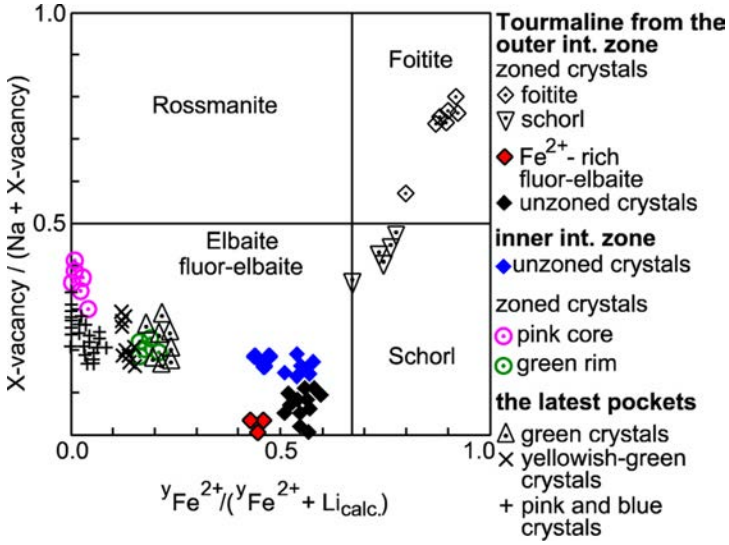

Figure 8. Classification of tourmaline compositions of generations 1, 2 and 3 from the Namacotche granitic pegmatite, Mozambique. Lines dividing the diagram represent 50% of the end-member components (DUTROW & HENRY, 2000). This diagram is also helpful for the interpretation of tourmalines.

7.3. Generation 3

The generation 3 consists of fluor-elbaite crystals from late units. They have $^{Y}Fe^{2+}/(^{Y}Fe^{2+}+Li_{calc.})$ values ranging between 0.23 and 0 (Fig. 8). The cycles a, b and c were distinguished:

The crystals of the cycle a have values of 0.18-0.23 for this ratio. They are dark green and green in color (Fig. 5C1). Most crystals are unzoned, but a few have an alternating slightly darker zone and slightly lighter zone in a BSE image (Fig. 7b). The lighter zone has higher $^{Y}Fe^{2+}$ and F contents than the darker zone, but the differences in contents of both zones are small (Table 3).

The crystals of the cycle b have $^{Y}Fe^{2+}/(^{Y}Fe^{2+}+Li_{calc.})$ values ranging from 0.16 to 0.12. They are yellowish green to green in color (Fig. 5C2). Most crystals are unzoned. Rare cat's eye crystals present a darker core and a lighter rim in a BSE image (Fig. 7c). The rim has slightly higher Mn, $^{Y}Fe^{2+}$, F contents and lower ^{Y}Al content than the core (Fig. 11, Table 3). The differences between contents from core and rim are small. These crystals are progressively zoned in BSE images. The variability within the cycle b is better described by the exchange vector $(LiOH)_2\ (AlO_2)^{-1}$ (Fig. 9a, c).

The crystals of the cycle c have $^{Y}Fe^{2+}/(^{Y}Fe^{2+}+Li_{calc.})$ values ranging between 0.079 and 0. A few pink crystals become discoloured towards the + c pole of the tourmaline. A sample contains an unzoned cat's eye and extends to the most fibrous part which is broken and may have been developed at the + c pole of tourmaline (Dutrow and Henry, 2016). The reversely zoned fibrous crystal has a darker rim containing a higher ^{Y}Al content and lower Mn and $^{Y}Fe^{2+}$ contents than the lighter core (Table 3), but the differences between both zones are also small.

The rare blue cat's eye crystals are unzoned. The variability within the cycle c is better described by the exchange vector $Li(OH)_2(AlO_2)_{-1}$ (Fig. 9a, c). In general, within the cycle c, the Li content increases and $^{Y}Fe^{2+}$ content and $^{Y}Fe^{2+}/(^{Y}Fe^{2+}+Li_{calc.})$ decrease (Figs. 8, 9, Table 3).

From the cycle a to the cycle b and the cycle c, Fe^{2+} content and $^{Y}Fe^{2+}/(^{Y}Fe^{2+}+Li_{calc.})$ value decrease and in general, Li content is higher in the cycle c than in the other cycles (Figs. 8, 9a; Table 3).

8. DISCUSSION

Tourmaline crystals occur in the wall zone, border zone, outer intermediate zone and inner intermediate zone (Table 1). Those of outer intermediate zone and inner intermediate zone were studied and they correspond to the generations 1 and 2. They are associated with very big spodumene crystals, which cross from the border zone to the intermediate zone.

8.1. The origin of the generation 1

Progressively zoned crystals of the generation 1 from outer intermediate zone, range from foitite - schorl in the inner core, to schorl at the outer core. The Fe-rich fluor-elbaite rim (Fig. 7a) and other unzoned Fe-rich F-elbaite compositions, from the same pegmatite zone and also from the inner intermediate zone, define linear fractionation trends, characterized by a decrease in the values of $^{Y}Fe^{2+}/(^{Y}Fe^{2+}+Li_{calc.})$, X-vacancy/(Na+X-vacancy) and $^{Y}Fe^{2+}$ content and an increase in $Li_{calc.}$ content (Figs. 8, 9a, Table 2). This suggest a magmatic fractionation of a (Al, Li, B)-rich pegmatite melt.

However, at the inner intermediate zone of the pegmatite, the chemical composition of the black Fe-rich fluor-elbaite rim (in a BSE image), showing a sharp contact with the schorl outer core (Fig. 7a) and some analyses of the Fe-rich fluor-elbaite crystal (in disequilibrium) have the lowest $^{Y}Fe^{2+}/(^{Y}Fe^{2+}+Li_{calc.})$ values and $^{Y}Fe^{2+}$ content. They are

plotted outside the linear trends (Figs. 8, 9a, Table 1), suggesting that they may have been hydrothermally affected or have a hydrothermal origin. In general, the Fe-rich composition is attributed to a crystallization coexisting with a Fe-rich aqueous fluid (e.g. Francis *et al*., 1999).

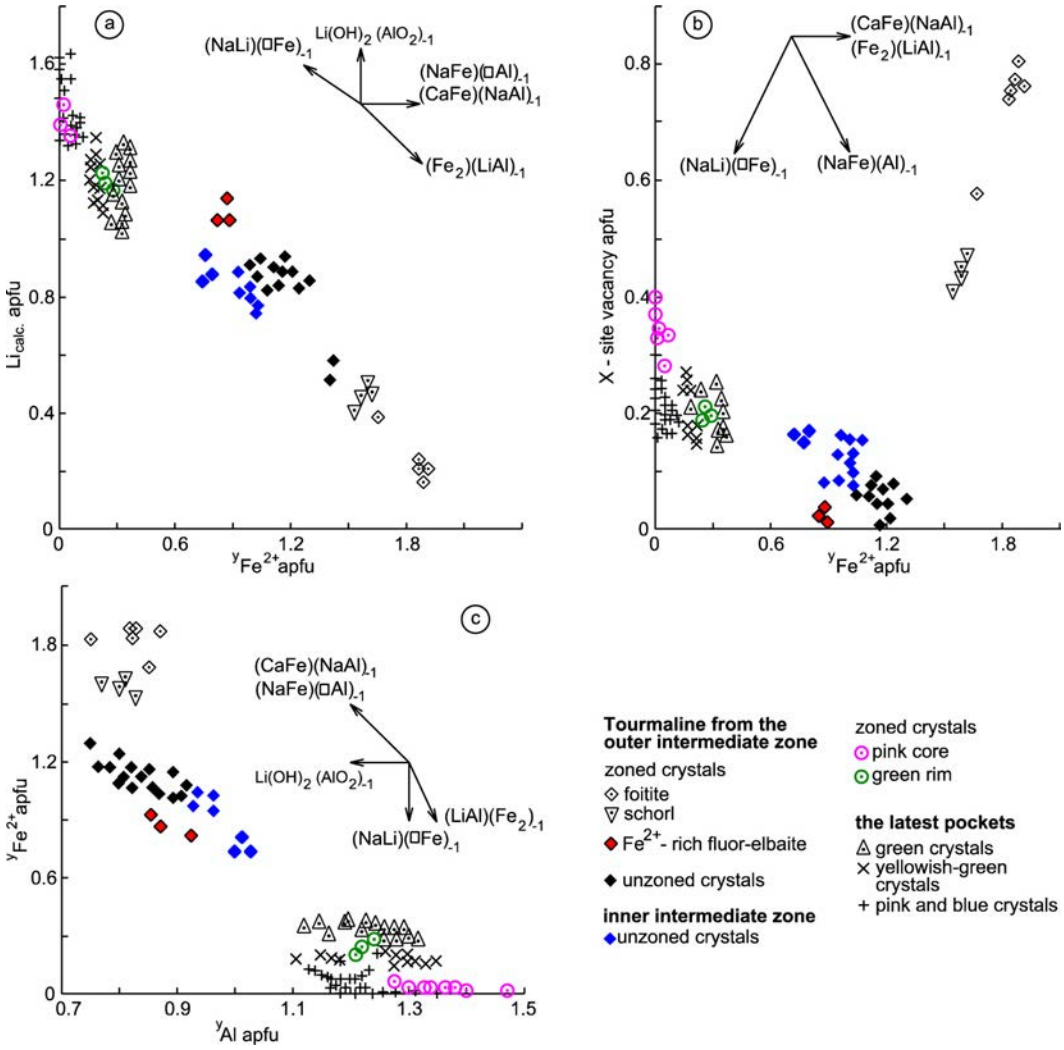

Figure 9. Diagrams showing the evolutions within each tourmaline generation from the Namacotche granitic pegmatites, Mozambique. a. Li vs $^{Y}Fe^{2+}$; b. X-site vacancy vs $^{Y}Fe^{2+}$; c. $^{Y}Fe^{2+}$ vs ^{Y}Al.

8.2. The origin of the generation 2

The watermelon, zoned, fluor-elbaite crystals of the generation 2 from the inner intermediate zone have a pink core, which has lower $^{Y}Fe^{2+}/(^{Y}Fe^{2+}+Li_{calc.})$ value, Fe^{2+} content and higher ^{Y}Al, Li, X-vacancy contents when compared to the Fe-rich fluor-elbaite in equilibrium of the generation 1, from the outer intermediate zone of the pegmatite. A compositional gap occurs between them (Figs. 8, 9, Table 2). This core is interpreted as hydrothermal. In the watermelon crystals, the rim has higher $^{Y}Fe^{2+}$, F, Na

contents, $^{Y}Fe^{2+}/(^{Y}Fe^{2+}+Li)$ value and lower $Li_{calc.}$ and X-site vacancy contents and X-vacancy/(Na+X-vacancy) value than the core (Figs. 8, 9, 10 and Table 2).

A gap between core and rim compositions (Figs. 8, 9, 10), indicate that the rim is an overgrowth and hydrothermal. The green fluor-elbaite rim is due to a late increase in Fe (Foord, 1977). As the rim has higher Na and F contents than the core, the increase in Fe in the rim is probably related to some internal source.

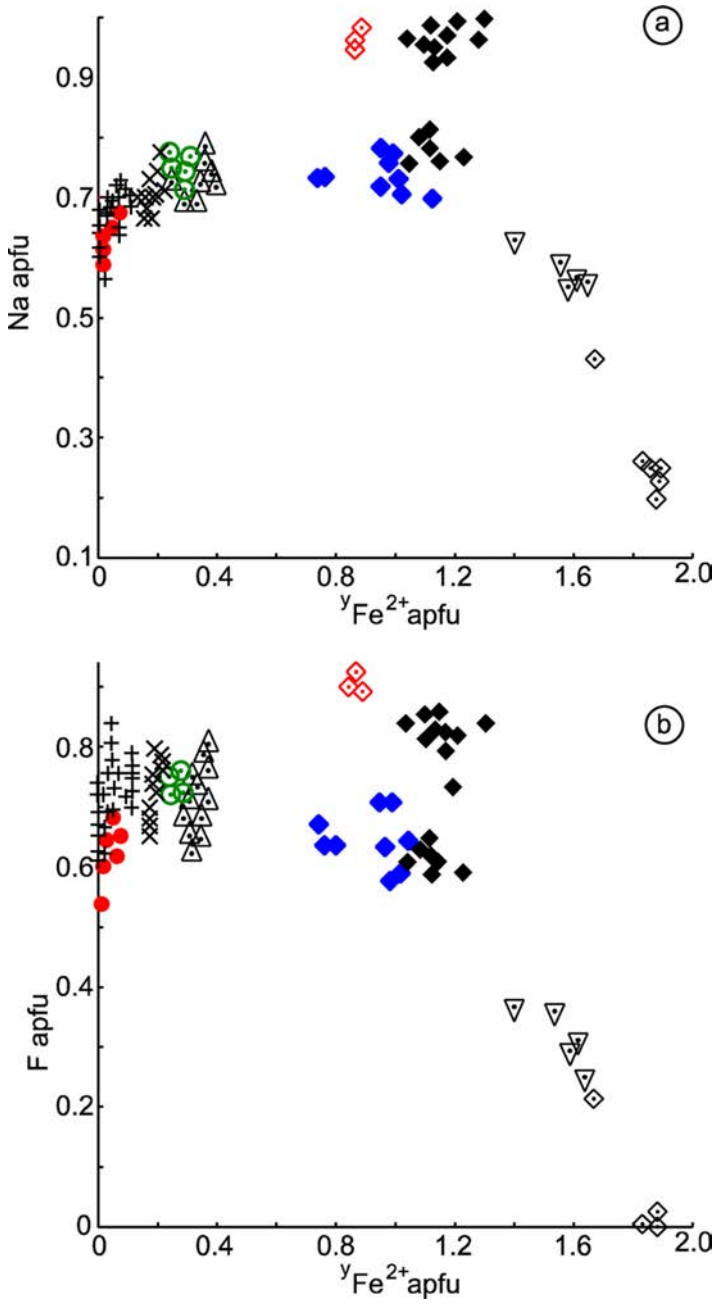

Figure 10. Compositional variation of tourmalines from Namacotche granitic pegmatite, Mozambique, in what concerns apfu(s) of Na/Fe (a) and F/Fe (b). Symbols as in Fig(s). 8 and 9.

8.3. The origin of the generation 3

The fluor-elbaite crystals of the generation 3 occur in sheared breccia blasts and clasts which may contain early tourmaline crystals, but intergrowths of late tourmaline with early minerals were not found. Clasts and blasts occur in a clay-cookeite matrix. The tourmaline crystals are mainly unzoned and of gem quality. Elbaite is the most common gem species as in SIMMONS (2014).

The $^{Y}Fe^{2+}$ content decreases from dark green to green crystals of the cycle a to yellowish green to green crystals of the cycle b and blue and pink crystals of the cycle c (Fig. 5C1-C4). The change in color is due to a decrease in $^{Y}Fe^{2+}$ content (Fig. 9a) (FOORD, 1977). The $^{Y}Fe^{2+}/(^{Y}Fe^{2+}+Li_{calc.})$ ratio also decreases from the cycle a (0.23-0.18) to the cycle b (0.16-0.12) and the cycle c (0.079-0) and generally Li content is higher in the cycle c (Figs. 8, 9a). The gemmy tourmaline crystals of the generation 3 developed in a hydrothermal pegmatite environment at low temperatures (280-150 ºC). Their fluor-elbaite compositions depend mainly on the fluid-rich hydrothermal environment (DUTROW & HENRY, 2016).

However, some crystals mainly of the cycle a may have resulted from dissolution of previously crystallized tourmalines, which were destabilized by influxes of fluids and came into local equilibrium (e.g. DUTROW & HENRY, 2000).

A replacement texture forms, because late fluids were in chemical disequilibrium and reacted with early-crystallized tourmaline crystals (DUTROW & HENRY, 2000; HENRY *et al*., 2002; TINDLE *et al*., 2002; ZHANG *et al*., 2008). The dissolved tourmalines will be from the pegmatite zone more stongly affected by shear.

Spodumene clasts associated with tourmaline crystals occur in the intermediate zone of the pegmatite and in sheared breccia clasts with a clay-cookeite matrix. Therefore, the dissolved tourmalines will be from the intermediate zone, particularly the magmatic tourmaline crystals of the generation 1 from the outer and inner intermediate zones. The fact that the hydrothermal fluor-elbaite crystals of the generation 2 from the inner intermediate zone have a similar core composition to that of fluor-elbaite from the cycle c and a rim composition close to those of cycles a and b (Figs. 8, 9) indicates that it was not previously dissolved. The growth of tourmaline started again when the fluids were saturated in the necessary components. Some of the boron for the new growth may have been provided by dissolution of previous tourmaline (DUTROW & HENRY, 2000).

As there is a chemical evolution of tourmaline composition from the cycle a to the cycle b and the cycle c with decrease in $^{Y}Fe^{2+}$ content $^{Y}Fe^{2+}/(^{Y}Fe^{2+}+Li_{calc.})$ value and increase in Li content (Figs. 8, 9a), the fluids giving way to their crystallizations were undergoing fractionation during hydrothermal crystallization at 280-150 ºC, associated with at least three shear deformation cycles.

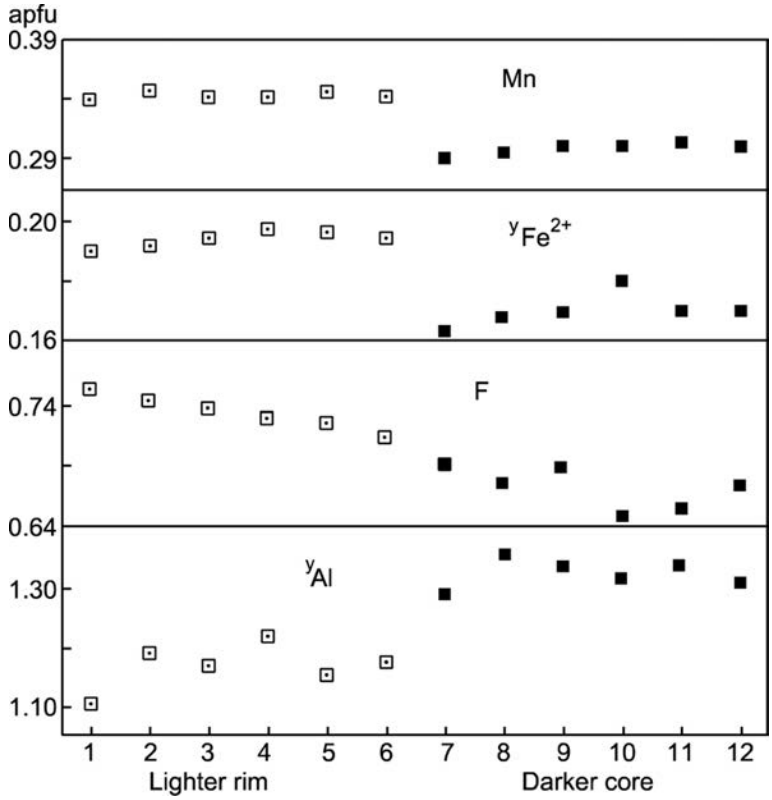

Figure 11. Compositional traverses across slightly zoned fluor-elbaite crystal of the generation 3 from the Namacotche granitic pegmatite, Mozambique.

9. CONCLUSIONS

The main findings of this study about tourmalines in the Namacotche, Li-Cs-Ta granitic pegmatite group are the following:

(1) the distinction between magmatic tourmalines and hydrothermal tourmalines;

(2) the generation 1 is magmatic and derived by fractionation of a (Al, Li, B)-rich pegmatite melt;

(3) the generation 2 is hydrothermal and consists of crystals with a core and an overgrowth;

(4) the generation 3 consists of hydrothermal gem tourmaline crystals in sheared breccia blasts and clasts with a clay-cookeite matrix.

Their fluor-elbaite compositions are mainly due to the fluid-rich hydrothermal environment associated with shear deformation cycles. The best gem quality is achieved in shear and hydrothermal related, blast and clasts, related to late, low temperature, crystallization and a generation of tourmaline recycling.

REFERENCES

Aquater (1983) Cartografia geológica e prospecção mineira e geoquímica nas províncias de Nampula e Zambézia, I, II, III. Relatório Final. *Unp. Report. DNG Library reference Nº 1244, Maputo*.

Bosi, F., Lucchesi, S. (2007) Crystal chemical relationship in the tourmaline group: structural constraints on chemical variability. *American Mineralogist* 92, 1054–1063.

Braga, M., Leal Gomes, C., Duplay, J., Paquet, H. (2008) Clay minerals in the Namacotche Pegmatite Group from Zambezia Province, Mozambique: main constituents of late stage secondary paragenesis. *Clay Minerals* 43, 513–529.

Černý, P. (1982) Anatomy and classification of granitic pegmatites. *In Granitic Pegmatites in Science and Industry (P. Černý, ed.). Mineral. Assoc. Can., Short Course Handbook* 8, 1–39.

Černý, P., Ercit, T.S. (2005) The classification of granitic pegmatites revisited. *Canadian Mineralogist* 43, 2005–2026.

Dirlam, D.M., Laurs, B.M., Pezzotta, F., Simmons, W.B. (2002) Liddicoatite tourmaline from Anjanabonoina, Madagascar. *Gems & Gemology* 38, 28–53.

Dutrow, B.L., Henry, D.J. (2000) Complexy zoned fibrous tourmaline, Cruzeiro mine, Minas Gerais, Brazil: A record of evolving magmatic and hydrothermal fluids. *Canadian Mineralogist* 38, 131–143.

Dutrow, B.L., Henry, D.J. (2016) Fibrous tourmaline: a sensitive probe of fluid compositions and petrologic environments. *Canadian Mineralogist* 54, 311–335.

Foord, E.E. (1977) The Himalaya dike system, Mesa Grande District, San Diego County, California. *Mineral Record* 8, 461–474.

Francis, C.A., Dyar, M.D., Williams, M.L., Hughes, J.M. (1999) The occurrence of crystal structure of foitite from a tungsten-vein at Copper Mountain, Taos County, New Mexico. *Canadian Mineralogist* 37, 1431–1438.

Hawthorn, F.C., Henry, D.J. (1999) Classification of minerals of the tourmaline group. *European Journal of Mineralogy* 11, 201–215.

Henry, D.J., Dutrow, B.L., Selverstone, J. (2002) Compositional asymmetry in replacement tourmaline – an example from the Tauern Window, East Alps. *Geological Materials Research* 4, 1–18.

Henry, D.J., Novák, M., Hawthorne, F.C., Ertl, A., Dutrow, B.L. Uher, P., Pezzota, F. (2011): Nomenclature of the tourmaline – subgroup minerals. *American Mineralogitst* 96, 895–913.

Leal Gomes C. (2003a) As paragéneses correspondentes à mineralização em gemas dos pegmatitos LCT do Alto Ligonha-Mozambique (Análise dos locais chave, Nahia, Nahipa e Namacotche). *Actas IV Congresso Ibérico de Geoquímica*, Coimbra, 199–201.

Leal Gomes, C. (2003b) O papel dos fenómenos de evolução tardia na génese de gemas pegmatíticas – ilações da análise paragenética em pegmatitos LCT do Alto Ligonha

(Moçambique). *A Geologia de Engenharia e os Recursos Geológicos*, Coimbra, Imprensa da Universidade, vol. II, 217–228.

Leal Gomes, C., Dias, P., Guimarães, F., Marques, J., Ferreira, J. (2006) Contrasting styles of Bi mineralization. Equilibrium and evolution in Zambezia Pegmatite Province, Mozambique. *Proc. 21st Colloq. Afric. Geol.*, *CAG Maputo*, 3.

Leal Gomes, C., Marques, J., Dias, P., Costa, J.C. (2008) Análise descritiva das unidades portadoras de mineralização tantalífera em pegmatitos do sul da província Zambeziana (Moçambique). *Proc. 5º Cong. Luso-Moçambicano de Engenharia, 2º Cong. Engenharia de Moçambique, Maputo*, 1–23.

Peretti, A., Bieri, W.P., Reusser, E., Hametner, K. (2009) Chemical variations in multicolored "Paraiba-type" tourmalines from Brazil and Mozambique. Implications for origin and authenticity determination. *Contributions to Gemology* 9, 77 p.

Simmons, W.B. (2014) Gem-bearing pegmatites. *In Geology of Gem Deposits*, L.A. Groat (ed.), second edition, 9, 257–299. Short Course Series, vol. 44, Tucson, Arizona.

Simmons, W.B., Pezzotta, F., Shigley, J.E., Beurlen, H. (2012) Granitic pegmatites as sources of colored gemstones. *Elements* 8, 281–287.

Simmons, W.B., Webber, K.L., Falster, A.U., Nizamaff, J.W. (2001) Gem tourmaline chemistry and paragenesis. *Australian Gemmologist* 21, 24–29.

Tindle, A.G., Breaks, F.W., Selway, J.B. (2002) Tourmaline in petalite-subtype granitic pegmatites: evidence of fractionation and contamination from the Pakeagama Lake and Separation Lake areas of northwestern Ontario, Canada. *Canadian Mineralogist* 40, 753–788.

Wilson, B.S. (2014) Colored gemstones from Canada. In L.A. Groat (ed.). Geology of Gem Deposits, second edition, Short Course Series, vol. 44, chap. 11, 375–405, Tucson, Arizona.

Zhang, A.C., Wang, R.C., Jiang, S.Y., Hu, H. (2008) Chemical and textural features of tourmaline from the spodumene-subtype koktokay nº 3 pegmatite, Altai, Northwestern China: A record of magmatic to hydrothermal evolution. *Canadian Mineralogist* 46, 41–58.